# Massive radius–dependent flow slippage in carbon nanotubes

Eleonora Secchi[1], Sophie Marbach[1], Antoine Niguès[1], Derek Stein[1,2], Alessandro Siria[1] & Lydéric Bocquet[1]

Measurements and simulations have found that water moves through carbon nanotubes at exceptionally high rates owing to nearly frictionless interfaces[1-4]. These observations have stimulated interest in nanotube-based membranes for applications including desalination, nano-filtration and energy harvesting[5-10], yet the exact mechanisms of water transport inside the nanotubes and at the water–carbon interface continue to be debated[11,12] because existing theories do not provide a satisfactory explanation for the limited number of experimental results available so far[13]. This lack of experimental results arises because, even though controlled and systematic studies have explored transport through individual nanotubes[7-9,14-17], none has met the considerable technical challenge of unambiguously measuring the permeability of a single nanotube[11]. Here we show that the pressure-driven flow rate through individual nanotubes can be determined with unprecedented sensitivity and without dyes from the hydrodynamics of water jets as they emerge from single nanotubes into a surrounding fluid. Our measurements reveal unexpectedly large and radius-dependent surface slippage in carbon nanotubes, and no slippage in boron nitride nanotubes that are crystallographically similar to carbon nanotubes, but electronically different. This pronounced contrast between the two systems must originate from subtle differences in

the atomic-scale details of their solid–liquid interfaces, illustrating that nanofluidics is the frontier at which the continuum picture of fluid mechanics meets the atomic nature of matter.

Measuring the pressure-driven flow of water through individual carbon nanotubes (CNTs) and boron nitride nanotubes (BNNTs) with well-defined radii (R_t) and lengths (L_t) requires overcoming two considerable challenges. First, when R_t decreases to the nanoscale, the flow rate through a tube drops too rapidly for even state-of-the-art flow-rate measurements to detect. Flow rates as low as a few picolitres per second have been measured through single nanocapillaries[18], but such a rate is still about three orders of magnitude higher than the sensitivity required to probe mass flow through a single nanotube. Our approach avoids this problem by focusing instead on the flow that a fluid jet entrains outside a nanotube (see Fig. 1) and on the scaling property of the jet hydrodynamics[19]. The external flow is characterized by a driving force F_P that originates in the fluid momentum transfer at the tube opening[20,21] and scales linearly with R_t, so the flow velocities remain measurably large even when R_t shrinks to nanometre-scale dimensions. The second challenge is fabricating an experimental system for manipulating and using a single nanotube, in the form of a nanofluidic needle with a single nanotube protruding from the tip. To do this, we adapted a technique for selecting and manipulating nanotubes of known length
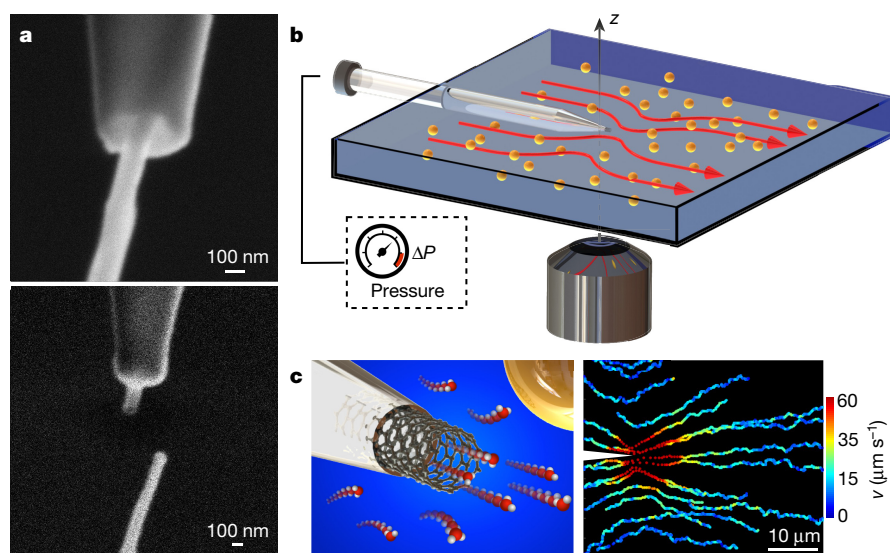
Figure 1 | Nanojet experimental set-up. a, SEM image of a CNT insertion into a nanocapillary (top) and after sealing (bottom). The CNT has dimensions of $(R_t, L_t) = (50\,\mathrm{nm}, 1{,}000\,\mathrm{nm})$. **b**, Sketch of the fluidic cell used to image the Landau–Squire flow set-up by nanojets emerging from individual nanotubes. Red arrows represent the Landau–Squire flow in the reservoir; orange spheres are tracer particles; z is the optical axis. **c**, Left, sketch of a nanotube protruding from a nanocapillary tip. The flow of water molecules emerging from the nanotube is probed by the tracer particles. Right, trajectories of individual colloidal tracers in a Landau–Squire flow field in the outer reservoir. The colour scale quantifies the velocity v of the tracer particles. The flow is driven by a nanojet from a CNT with dimensions of $(R_t, L_t) = (33\,\mathrm{nm}, 900\,\mathrm{nm})$, with $\Delta P = 1.7\,\mathrm{bar}$. Both reservoirs contained water with $10^{-2}\,\mathrm{M}$ KCl.

[1]Laboratoire de Physique Statistique, Ecole Normale Supérieure, PSL Research University, 75005 Paris Cedex 05, France. [2]Physics Department, Brown University, Providence, Rhode Island 02912, USA.

and diameter with a nanomanipulator operating inside a scanning electron microscope (SEM)[9]; see Supplementary Methods 1 and Supplementary Video 1. We guided a nanotube into the tip of a laser-pulled glass nanocapillary with an orifice in the range 250–350 nm. The dimensions of the nanotubes were determined by ionic transport measurements and by electron microscopy (see Supplementary Methods 2 and 4). For this study we tested five different CNTs with dimensions (in nanometres) of $(R_t, L_t) =$ (15, 700), (17, 450), (33, 900), (38, 800) and (50, 1,000), and three different BNNTs with dimensions (in nanometres) of $(R_t, L_t) =$ (23, 600), (26, 700) and (7, 1,300); see Supplementary Methods 2 and 4 and Supplementary Table 1.

The nanotube at the tip of the glass capillary bridged two macroscopic fluid reservoirs: one inside the capillary and another in the wide, transparent flow cell into which the capillary was placed (see Fig. 1b and Supplementary Methods 3). We filled both reservoirs with potassium chloride (KCl) solutions of a chosen concentration C_s and controlled pH, and seeded the flow cell with 500-nm polystyrene tracer particles. We then applied a pressure drop ΔP to the capillary and tracked the resulting motion of the tracers under a microscope (see Fig. 1b) to map the velocity profile of the flow (see Figs 1c and 2). Flow measurements were performed with salt concentration $C_s = 10^{-3}\,\mathrm{M}$ or $C_s = 10^{-2}\,\mathrm{M}$. Low salinity is required during the tracking experiments to prevent salt-induced colloid aggregation.

Ag/AgCl electrodes inserted into either reservoir were used to measure the ionic conductance across the nanotube before and after each fluidic experiment to ensure the integrity of the device, as well as to obtain information on the dimensions and the surface charge density

of the nanotube (see Supplementary Methods 4). These electrodes were grounded during flow measurements.

Owing to the needle geometry of the system, the pressure-driven flow through the nanotube sets up a flow in the outer reservoir called a Landau–Squire nanojet[18,20,21]. The Landau–Squire solution of the Navier–Stokes equations at low Reynolds number predicts radial and angular components of the flow velocity of $v_r = \frac{F_P}{4\pi\eta}\frac{\cos\theta}{r}$ and $v_\theta = -\frac{F_P}{8\pi\eta}\frac{\sin\theta}{r}$, respectively, where r is the radial distance from the tip, θ is the angle relative to the symmetry axis of the jet and η is the viscosity[20]. F_P is the driving force of the jet applied at the origin. Figure 2a, b shows that our measurements of the flow field around single nanotubes agree well with the Landau–Squire prediction. The inset of Fig. 2b further highlights the long-range $1/r$-dependence of the Landau–Squire flow, which extends over tens of micrometres despite the nanometre-scale size of the source of the flow.

From our analysis of the Landau–Squire flow, we extracted experimental values of F_P for each nanotube and ΔP. The results, presented in Fig. 2c, show a linear relationship between F_P and ΔP. To gain insight into the permeability of the nanotubes, we begin by observing that the mass flow rate and F_P are both proportional to ΔP and, hence, proportional to one another. The viscous origin of F_P at low Reynolds numbers as well as dimensional considerations motivate the definition $F_P = \alpha\eta R_t v_{NT}$, where $\alpha = \mathcal{O}(1)$ is a geometry-dependent numerical prefactor and v_{NT} is the average fluid velocity inside the nanotube. The permeability of the tube k_{NT} is defined by $v_{NT} = \frac{k_{NT}}{\eta}\frac{\Delta P}{L_t}$. Combining these expressions, F_P, k_{NT} and ΔP are related by $F_P(\Delta P) = \frac{\alpha R_t k_{NT}}{L_t}\Delta P$.
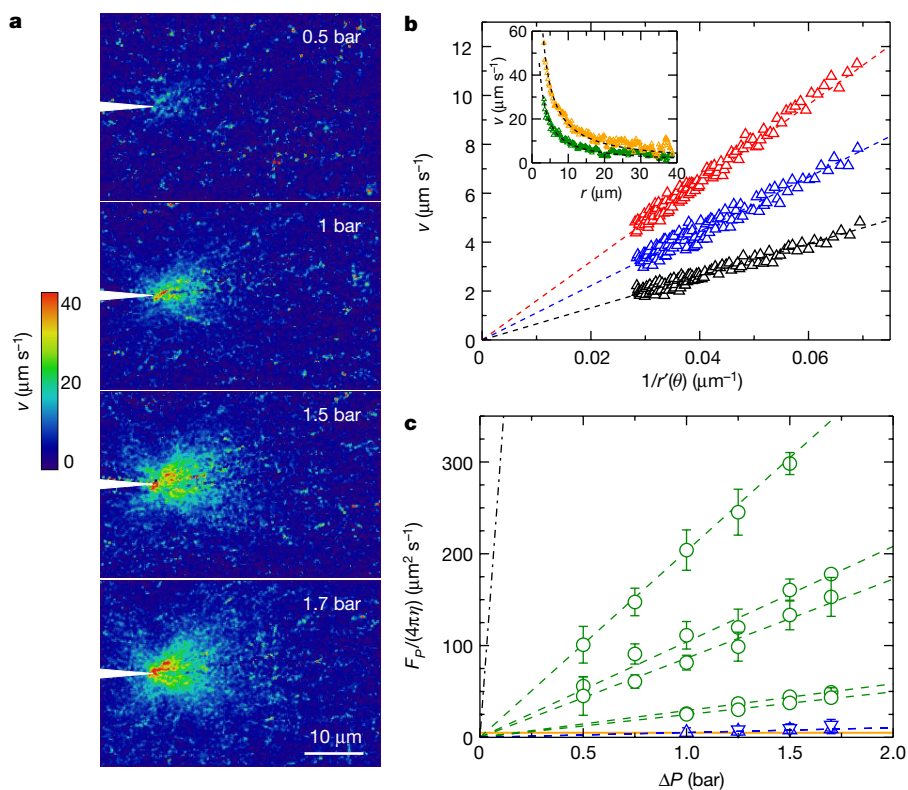
Figure 2 | Measurement of Landau–Squire flows driven from nanotubes. a, Maps of the velocity field near a CNT with $(R_t, L_t) = $ (33 nm, 900 nm) for various ΔP as indicated ($C_s = 10^{-2}\,\mathrm{M}$ and pH 6). **b**, Magnitude of mean particle velocity v as a function of $r'(\theta) = 2r/\sqrt{1 + 3\cos^2\theta}$ for $\Delta P = 0.5$ bar (black), $\Delta P = 1$ bar (blue) and $\Delta P = 1.5$ bar (red). Dashed lines are fits of the Landau–Squire prediction. Inset, particle velocity along the jet axis ($\theta = 0$) versus distance from the nanotube, for $\Delta P = 0.75$ bar (green) and $\Delta P = 1.7$ bar (orange); the dashed line is a $1/r$ fit. **c**, Dependence of $\frac{F_P}{4\pi\eta}$ on ΔP for CNTs (green circles) and BNNTs (blue triangles). CNT dimensions (in nanometres) are,

from top to bottom, $(R_t, L_t) = $ (50, 1,000), (33, 900), (38, 800), (15, 700) and (17, 450); BNNT dimensions (in nanometres) are $(R_t, L_t) = $ (26, 700) and (23, 600). The salt concentration is $C_s = 10^{-3}\,\mathrm{M}$, except for the 33-nm CNT, which was studied at both $C_s = 10^{-3}\,\mathrm{M}$ and $C_s = 10^{-2}\,\mathrm{M}$ without a detectable difference. Dashed green lines are linear fits from which the permeability was calculated. The orange line indicates the lowest detectable flow strength. The black dashed line corresponds to the results of a control experiment using a nanocapillary without a nanotube (see Supplementary Methods 5). Error bars correspond to the uncertainty in the slope in **b**, estimated from at least three measurement replicates at each ΔP.
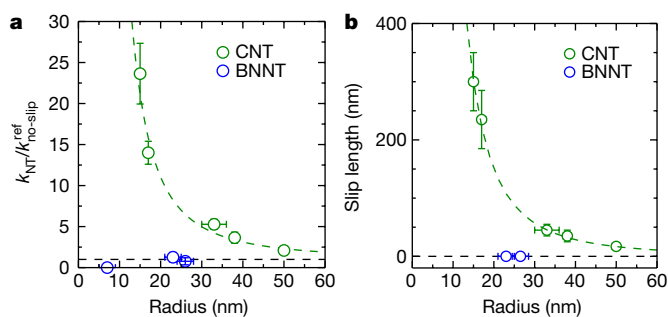
Figure 3 | Permeability and slip length of individual CNTs and BNNTs.
a, Normalized permeability ($k_{NT}/k_{no\text{-}slip}^{ref}$) of CNTs (green) and BNNTs (blue) as a function of nanotube radius R_t. The permeability of the BNNT with $R_t = 7$ nm was below the experimental detection limit and is indicated as $k_{NT} = 0$ for completeness. Error bars correspond to the experimental errors on F_P. **b**, Dependence of the experimentally determined slip length inside CNTs (green) and BNNTs (blue) on R_t. Error bars correspond to the uncertainty in the permeability. Salt concentration is $C_s = 10^{-3}$ M, except for the 33-nm CNT, which was studied at both $C_s = 10^{-3}$ M and $C_s = 10^{-2}$ M without a detectable difference. Iin both panels, the horizontal dashed lines indicate the no-slip prediction ($k_{NT}/k_{no\text{-}slip}^{ref} = 1$) and the green dashed lines are guides to the eye. The error bars on the radius correspond to the experimental uncertainty in the electric characteristics (see Supplementary Methods 2 and 4). The values of the slip lengths are reported in Supplementary Tables 2 and 3.

According to this equation, the slope of the plots in Fig. 2c provides an estimate of the nanotube permeability, so we can already see that the permeability of CNTs is greatly enhanced as compared with BNNTs. But, to properly quantify the permeabilities, we need to know the value of α. We calculated α from the precise relationship between F_P, v_{NT} and ΔP that we obtained by numerically solving the full hydrodynamic Landau–Squire flow. Furthermore, because α could be sensitive to details of the geometry of the nanotube and the tip, we repeated our calculations for every nanotube device, taking in account its particular geometry as measured by SEM (see Supplementary Methods 6). This exhaustive study, which combines numerical hydrodynamic calculations with experimental benchmarking using nanocapillaries, is summarized in Supplementary Methods 5. Our study showed that $\alpha \approx 0.3$ for the nanotube devices considered in Fig. 2a, b, with only small variations between nanotubes. Having removed all uncertainty from the value of α, we obtained accurate values for k_{NT} from the experimental dependence of F_P on ΔP. Figure 3a presents the dependence of k_{NT} on R_t for every nanotube. The permeabilities are normalized by a simple no-slip reference, $k_{no\text{-}slip}^{ref} = R_t^2/8$, corresponding to a nanotube of the same size with a no-slip boundary condition at its surface. Note that the flow from the smallest BNNT tube, with $R_t = 7$ nm, was below the detection limit.

We attribute the enhanced permeability of the CNTs to hydrodynamic slippage at the carbon surface[12,13,22,23]. The fundamental way to account for this is to introduce a slip length b and to apply Navier's slip boundary condition to the fluid at the nanotube surface. We included the slip condition in our numerical analysis of the hydrodynamics of each nanotube device and obtained experimental b values by matching the computed flow rate enhancement due to surface slippage with the measured permeability data in Fig. 3a (see Supplementary Methods 6). This analysis, which uses the geometry of each nanotube device and takes into account hydrodynamic entrance effects at the nanotube ends, offers the most accurate estimation of b possible. The permeability and b can also be quantitatively obtained from an analytical model of hydrodynamic resistances in series, using the Sampson formula to account for both Poiseuille flow with slippage inside the nanotube and entrance effects[24]; see Supplementary Tables 2 and 3.

The peculiar nature of the water–carbon interface inside CNTs is revealed in Fig. 3b, which presents the experimentally determined slip

length as a function of R_t. A first key observation is that the slip length is strongly radius-dependent, reaching 300 nm inside the smallest CNT investigated here. This observation allows us to resolve a long-standing debate regarding the large difference in permeabilities reported previously[2–4,25] using large-scale CNT membranes. The results of those studies are consistent with a decreasing permeability enhancement factor for larger nanotubes, and the range of slip lengths they report is fairly compatible with what we have measured. Our results also explain why the slip lengths measured previously inside CNTs were consistently much larger than the values measured on planar hydrophobic and graphite surfaces[13,26], for which b is typically a few tens of nanometres at most. From a theoretical perspective, the transport behaviour of water inside CNTs has been the subject of numerous studies, mostly using molecular dynamics simulations[12,13]. Radius-dependent slippage was predicted inside CNTs with $R_t < 10$ mn (refs 22, 23) and rationalized in terms of curvature-dependent friction[23]. The results presented here confirm the predicted trend, but the measured slip lengths far exceed the numerical predictions. This discrepancy suggests that molecular dynamics simulations do not represent the interfacial dynamics well at a quantitative level, echoing similar limitations encountered in studies of slippage at hydrophobic surfaces[13].

A second key feature of Fig. 3c is the vastly different behaviour of CNTs and BNNTs, with the latter showing no substantial slippage of water. The comparison is illuminating because CNTs and BNNTs have the same crystallography, but radically different electronic properties, with CNTs being semi-metallic and BNNTs insulating. That these nearly identical channels exhibit very different surface flow dynamics is unexpected: molecular dynamics simulations using semi-empirical interfacial parameters predict similar flow behaviour through CNTs and BNNTs[27,28]. More recent *ab initio* simulations predict that the friction of water on carbon surfaces is lower than on boron nitride surfaces[29], but even these predictions strongly underestimate the difference observed here. The stark differences in flow behaviour must therefore originate in subtle atomic-scale details of the solid–liquid interface, including the electronic structure of the confining material. A more detailed understanding will require a systematic theoretical investigation of physico-chemical factors that could affect surface friction, such as chemical surface dissociation or specific ion adsorption. Useful information could also be gained by measuring the slip behaviour in CNTs at high salt concentrations, a regime in which the surface charge of CNTs is expected to increase[15].

The unexpected slippage behaviour inside CNTs and BNNTs points to a hitherto not appreciated link between hydrodynamic flow and the electronic structure of the confining material. This opens up a new avenue for research that could bridge the gap between hard and soft condensed matter physics. We also expect that, with further improvements in sensitivity, the methods we have developed will enable the direct measurement of water transport through biological channels such as aquaporins.

1. Hummer, G., Rasaiah, J. C. & Noworyta, J. P. Water conduction through the hydrophobic channel of a carbon nanotube. *Nature* **414,** 188–190 (2001).
2. Majumder, M., Chopra, N., Andrews, R. & Hinds, B. J. Nanoscale hydrodynamics: enhanced flow in carbon nanotubes. *Nature* **438,** 44 (2005); erratum **438,** 930 (2005).
3. Holt, J. K. *et al.* Fast mass transport through sub-2-nanometer carbon nanotubes. *Science* **312,** 1034–1037 (2006).
4. Whitby, M., Cagnon, L., Thanou, M. & Quirke, N. Enhanced fluid flow through nanoscale carbon pipes. *Nano Lett.* **8,** 2632–2637 (2008).
5. Nair, R. R., Wu, H. A., Jayaram, P. N., Grigorieva, I. V. & Geim, A. K. Unimpeded permeation of water through helium-leak-tight graphene-based membranes. *Science* **335,** 442–444 (2012).
6. Joshi, R. K. *et al.* Precise and ultrafast molecular sieving through graphene oxide membranes. *Science* **343,** 752–754 (2014).
7. Park, H. G. & Jung, Y. Carbon nanofluidics of rapid water transport for energy applications. *Chem. Soc. Rev.* **43,** 565–576 (2014).
8. Liu, H. *et al.* Translocation of single stranded DNA through single-walled carbon nanotubes. *Science* **327,** 64–67 (2010).

9. Siria, A. *et al.* Giant osmotic energy conversion measured in a single transmembrane boron nitride nanotube. *Nature* **494,** 455–458 (2013).
10. Geng, J. *et al.* Stochastic transport through carbon nanotubes in lipid bilayers and live cell membranes. *Nature* **514,** 612–615 (2014).
11. Guo, S., Meshot, E. R., Kuykendall, T., Cabrini, S. & Fornasiero, F. Nanofluidic transport through isolated carbon nanotube channels: advances, controversies, and challenges. *Adv. Mater.* **27,** 5726–5737 (2015).
12. Whitby, M. & Quirke, N. Fluid flow in carbon nanotubes and nanopipes. *Nat. Nanotechnol.* **2,** 87–94 (2007).
13. Bocquet, L. & Charlaix, E. Nanofluidics, from bulk to interfaces. *Chem. Soc. Rev.* **39,** 1073–1095 (2010).
14. Lee, C. Y., Choi, W., Han, J.-H. & Strano, M. S. Coherence resonance in a single-walled carbon nanotube ion channel. *Science* **329,** 1320–1324 (2010).
15. Secchi, E., Niguès, A., Jubin, L., Siria, A. & Bocquet, L. Scaling behavior for ionic transport and its fluctuations in individual carbon nanotubes. *Phys. Rev. Lett.* **116,** 154501 (2016).
16. Qin, X., Yuan, Q., Zhao, Y., Xie, S. & Liu, Z. Measurement of the rate of water translocation through carbon nanotubes. *Nano Lett.* **11,** 2173–2177 (2011).
17. Lorenz, U. & Zewail, A. Observing liquid flow in nanotubes by 4D electron microscopy. *Science* **344,** 1496–1500 (2014).
18. Laohakunakorn, N. *et al.* A Landau–Squire nanojet. *Nano Lett.* **13,** 5141–5146 (2013).
19. Eggers, J. & Villermaux, E. Physics of liquid jets. *Rep. Prog. Phys.* **71,** 036601 (2008).
20. Landau, L. D. & Lifshitz, E. M. *Fluid Mechanics* Vol. 6 of *Course of Theoretical Physics* 81–83 (Pergamon, 1959).
21. Squire, H. B. The round laminar jet. *Q. J. Mech. Appl. Math.* **4,** 321–329 (1951).
22. Thomas, J. A. & McGaughey, A. J. H. Reassessing fast water transport through carbon nanotubes. *Nano Lett.* **8,** 2788–2793 (2008).
23. Falk, K., Sedlmeier, F., Joly, L., Netz, R. R. & Bocquet, L. Molecular origin of fast water transport in carbon nanotube membranes: superlubricity versus curvature dependent friction. *Nano Lett.* **10,** 4067–4073 (2010).
24. Sampson, R. A. On Stokes's current function. *Phil. Trans. R. Soc. A* **182,** 449–518 (1891).
25. Mattia, D., Leese, H. & Lee, K. P. Carbon nanotube membranes: from flow enhancement to permeability. *J. Membr. Sci.* **475,** 266–272 (2015).
26. Maali, A., Cohen-Bouhacina, T. & Kellay, H. Measurement of the slip length of water flow on graphite surface. *Appl. Phys. Lett.* **92,** 053101 (2008).
27. Suk, M. E., Raghunathan, A. V. & Aluru, N. R. Fast reverse osmosis using boron nitride and carbon nanotubes. *Appl. Phys. Lett.* **92,** 133120 (2008).
28. Hilder, T. A., Gordon, D. & Chung, S.-H. Salt rejection and water transport through boron nitride nanotubes. *Small* **5,** 2183–2190 (2009).
29. Tocci, G., Joly, L. & Michaelides, A. Friction of water on graphene and hexagonal boron nitride from ab initio methods: very different slippage despite very similar interface structures. *Nano Lett.* **14,** 6872–6877 (2014).

Author Contributions L.B. and A.S. conceived and directed the research. A.N. and A.S. designed and fabricated the nanotube devices. E.S and D.S. designed the fluidic cell. E.S. performed the measurements. The data were analysed by E.S., S.M. and L.B.; S.M. conducted the numerical analysis with input from the other authors. All authors contributed to the scientific discussions and the preparation of the manuscript.

Author Information Reprints and permissions information is available at www.nature.com/reprints. The authors declare no competing financial interests. Readers are welcome to comment on the online version of the paper. Correspondence and requests for materials should be addressed to L.B. (lyderic.bocquet@lps.ens.fr) and A.S. (alessandro.siria@lps.ens.fr).

Reviewer Information *Nature* thanks J. Eijkel and A. Michaelides for their contribution to the peer review of this work.